Strojniški vestnik - Journal of Mechanical Engineering 68(2022)12, 725-734
DOI:10.5545/sv-jme.2022.349
Original Scientific Paper
Received for review: 2022-08-29
Received revised form: 2022-10-26
Accepted for publication: 2022-11-03


# Multi-Objective Optimization of the Chebyshev Lambda Mechanism

Daniel Miler* – Dominik Birt – Matija Hoić
University of Zagreb, Faculty of Mechanical Engineering and Naval Architecture, Croatia

*Walking mechanisms are a solution for cases in which wheels are not applicable, such as uneven or stepped surfaces and surfaces with obstacles. Furthermore, it is possible to tailor mechanism footpaths to expected working conditions through optimization. Thus, in this paper, a mechanism optimization process was proposed, focusing on single-leg performance. Numerical Simulink calculations were used to determine objective function values, which were then input to a non-dominated sorting genetic algorithm (NSGA-II) for optimization. In each following generation, NSGA-II provided a new set of units for evaluation. The procedure was applied to the single leg of the Chebyshev lambda mechanism to better illustrate it, enabling a comprehensive analysis of candidates. Four objective functions (i.e., length in the x-direction, trajectory height variation, maximum foot acceleration, and foot speed fluctuation) were used to carry out a multi-objective optimization. The calculation time was approximately 2 s/unit.*

**Keywords: Chebyshev lambda mechanism, optimization, synthesis, walking mechanism**

**Highlights**
- *A procedure for the optimization of walking mechanisms was presented.*
- *Simscape mechanism model was embedded within the NSGA-II; approx. calculation time was 2 s per unit*
- *Four objective functions were used to optimize the Chebyshev lambda mechanism.*
- *The proposed procedure can be applied to other types of walking mechanisms.*

## 0 INTRODUCTION

Walking mechanisms imitate the leg motion of walking creatures and are comprised of linkages and joints. Despite their shortcomings compared to wheeled drives, including the lower efficiency, stride height variations, and higher complexity, they are useful in special applications [1]. Walking mechanisms can be used while traversing uneven or stepped surfaces [2] where wheeled mechanisms cannot be used. Also, they are applicable in regular flat surfaces with obstacles [3], e.g., a warehouse with sensitive cables on the floor or propelling devices through water via paddles [4]. Many types of walking mechanisms are available, each with a specific trajectory and number of joints and linkages. Thus, the mechanism type can be selected depending on the desired outputs. Examples include the Chebyshev lambda, Klann, and Jansen mechanisms [5] to [7].

The above-listed mechanisms can be applied in multiple ways, either using the default linkage values or optimizing them for a specific purpose. Komoda and Wagatsuma [5] compared the performances of the Chebyshev, Klann, and Jansen mechanisms regarding energy consumption and trajectory. It was found that the simplest of the three (Chebyshev) yielded the roughest trajectory, while the most complex one (Jansen) resulted in a finer trajectory and had higher efficiency. The authors concluded that walking mechanisms behave similarly to biological evolution based on such results. Moreover, Kim et al. [8] compared the performances of three walking mechanisms (i.e., four-bar, Klann, and Watt-I) using water running as a case. Following the kinematic analysis, the former two yielded higher propulsion.

Additionally, the same mechanism might have multiple purposes, given that it is reconfigurable, i.e., that linkage lengths can be varied during the operation. Sheba et al. [9] presented the reconfigurable Klann mechanism to generate various gait cycles: digitigrade locomotion, jam avoidance, step climbing, hammering, and digging. Foot trajectories were obtained analytically, and link dimensions and the total number of links were varied. Similarly, Nansai et al. [6] and [10] studied and designed a reconfigurable Jansen linkage to produce several gait types: digitigrade locomotion, obstacle avoidance, jam avoidance, step climbing, and drilling motion. Hence, it can be concluded that many mechanism types are used, while the linkage lengths are often varied, especially in reconfigurable mechanisms.

For this reason, the need to adapt the existing walking mechanisms to specialized engineering problems is evident. This problem can be easily solved via optimization, which will, in addition to ensuring a feasible solution, yield additional benefits for regular and reconfigurable mechanisms. Several studies were carried out on the optimization of walking

*Corr. Author's Address: University of Zagreb, Faculty of Mechanical Engineering and Naval Architecture, Ivana Lučića 5, 10002 Zagreb, Croatia, daniel.miler@fsb.hr

mechanisms, especially when developing novel types. For example, Desai et al. [11] presented an eight-link walking mechanism of the planar Peaucellier-Lipkin type. Once the mechanism geometry was outlined, the authors used the genetic algorithm to find the optimal linkage lengths. Variation in the foot path was used as the sole objective function and was minimized, while the transmission angle and stride height were limited. The results were verified experimentally.

Similarly, Erkaya [12] used the genetic algorithm to find the Jansen mechanism linkage lengths that will result in the minimum foot trajectory variations. While developing a legged closed-chain passive-locomotion platform, Wei et al. [13] optimized the foot trajectory. Two objectives were introduced, vertical variation and the longitudinal force between foot and ground. The multi-objective optimization was carried out via a weighted objective function.

A new mechanism optimization process simplifies the mechanism design and improves its outcomes. The non-dominated sorting genetic algorithm (NSGA-II) was used for optimization, while objective functions were evaluated through Simscape Multibody (Matlab subroutine). The mechanism's multi-objective optimization was carried out for three objective function pairs. Furthermore, boundary conditions were included based on Grashof's law to ensure feasibility. The utility of the optimization process was exhibited using the Chebyshev's lambda mechanism as an example. Its performance concerning the trajectory length (in $x$-direction), height variation, foot speed flux, and foot acceleration was assessed.

The primary scientific contribution of this paper is the optimization process; the numerical Simulink calculations were used to determine objective function values, which were then input to NSGA-II for optimization. In each following generation, NSGA-II provides a new set of units for the Simulink evaluation. The paper is outlined as follows: the problem and the associated optimization process were outlined in Section 2, along with design variables, objective functions, and boundary conditions. Algorithm settings were also provided. Further, the Simscape model of the mechanism was shown in Section 3. Next, the optimization process results were presented and discussed in Section 4, while Section 5 provided key findings and limitations of the presented work and a future outlook.

## 1 METHODS

The Chebyshev lambda mechanism is a simple four-bar linkage mechanism that converts the rotational motion into straight motion. Due to its low trajectory height variability, it is a suitable solution for walking mechanisms. In this paper, it was studied through optimization via the genetic algorithm and Simulink Multibody. Due to its symmetry, one-half of the mechanism was observed in this paper (see Fig. 1).

The multi-objective optimization of the mechanism was carried out using the genetic algorithm; the NSGA-II was used to find the optimal results (for more details, see Section 2.1). Four objective functions were used: length in the x-direction, trajectory height variation, speed fluctuation, and maximum acceleration. The latter two were observed for the output point of the mechanism (i.e., its foot). However, due to the complexity of analytical expressions and to obtain more comprehensive results, Simscape Multibody was used to obtain the values of objective functions numerically. Hence, objective functions and the associated Simscape calculation procedures were outlined in Section 2.2. The optimization process overview is shown in Fig. 2.

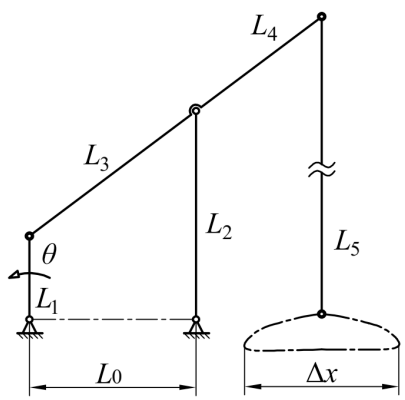


**Fig. 1.** *Chebyshev's Lambda mechanism – annotations*

The mechanism studied in this paper consists of five linkages, with linkages denoted $L_1$ to $L_5$ with default values of {100, 250, 250, 250, 1000} mm. The distance between the anchors was $L_0$ (see Fig. 1), with a default value of 200 mm. Linkages $L_1$ and $L_2$ were anchored, and $L_1$ served as the mechanism actuator. It should be added that both anchors are located at the same height. The sum of default linkage lengths $L_{SUM}$ = 2050 mm was used as an input parameter, while the lengths were varied (including $L_0$). Finally, the design variable vector was written as:

$$\mathbf{x} = \{L_0\ L_1\ L_2\ L_3\ L_4\}, \tag{1}$$

while $L_5$ was calculated by subtracting the design variable vector sum from the $L_{SUM}$. The values of

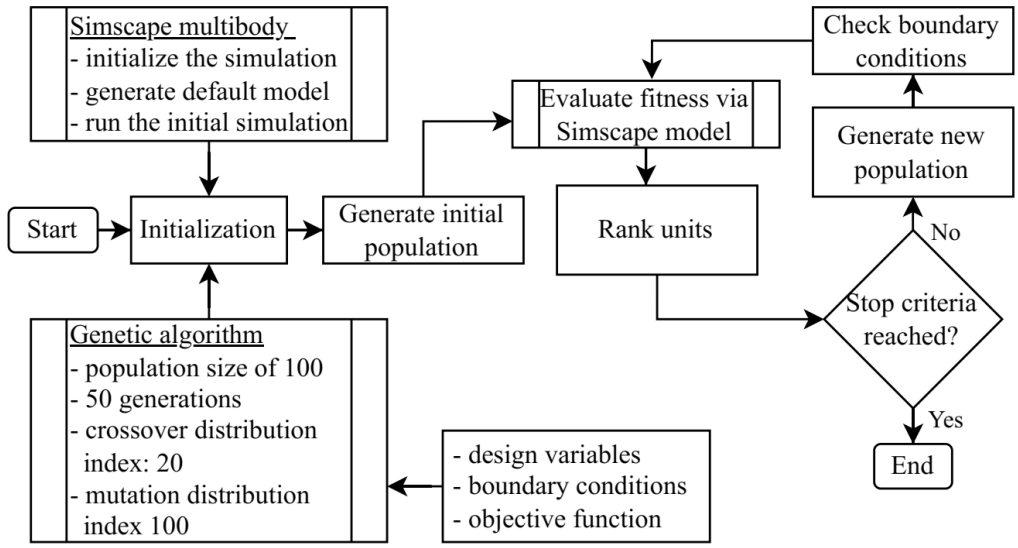


**Fig. 2.** *Optimization process overview*

design variables $L_0$, $L_1$, $L_2$, and $L_4$ were varied with respect to the default values used for this type of mechanism. Ranges were set to [0.9…1.1] of default values. This approach was not applied to $L_3$, as it was necessary to ensure that selected lengths would result in a mechanism that can be assembled for each unit within the population (i.e., mechanism feasibility). Thus, Grashof's criterion was used to find the $L_3$ boundary:

$$L_3 > L_0 + L_1 - L_2. \tag{2}$$

### 2.1 Optimization Algorithm Properties

Optimal solutions were found using the NSGA-II [14]. The NSGA-II is a non-dominated sorting genetic algorithm extensively used in engineering due to its ensured convergence and absence of sharing parameters [15]. As such, it was widely applied in multiple engineering fields, with examples including materials design [16], design of mechanical components [17], and energy consumption management [18].

The crossover and mutation rates were defined through the crossover distribution index and the mutation distribution index. Default values provided by the algorithm authors were used; 20 for the crossover and 100 for the mutation distribution index. It was also necessary to select the population size and the number of generations. The selected population size of 100 units was improved through 50 generations to retain reasonable computational time. Moreover, to ensure that the results are near the global optimal, the optimization procedure was verified by repeating the process using the significantly larger population size and the number of generations. The first verification was carried out by increasing the number of generations to 500 while keeping the population size constant. The second verification was the opposite; a large population size (1000 units) was used while the number of generations was kept constant. Finally, algorithm properties were the same for each of the observed objective function sets.

### 2.2 Calculating the Objective Function Values

As noted earlier, this study considered four objective functions: the length in the *x*-direction, trajectory height variation, foot speed fluctuation, and maximum foot acceleration. As shown in Fig. 1, the genetic algorithm exported the linkage lengths for each of the units in the population, which were then automatically imported into Simscape.

The Simscape mechanism model was developed as follows: the Chebyshev lambda mechanism consisting of linkages, joints, and anchors was modelled. Linkage properties were defined, including their cross-section and material properties; additionally, linkages were connected using pins, which were also fully defined. The relations between the linkages were achieved using joints, for which it was necessary to define degrees of freedom. Measurements were carried out at point 5 (mechanism foot), located on the free end of the linkage $L_5$ (Fig. 2). Its position, velocity, and acceleration were output for

each position during the cycle. The top-level schema of the Simscape model is shown in Fig. 3.

Simscape Multibody simulation was carried out next and provided all the necessary information; foot positions, velocities, and accelerations were calculated for the mechanism cycle. The resulting points were then used to obtain the values of objective functions. The stride cycle was discretized into 3024 points, and the leg foot positions and accelerations were calculated for each point. Hence, the calculation step was 0.12°.

### 2.2.1 Length in the x-Direction

Length in the x-direction (also denoted as Length Δx) was selected as the base objective and was thus considered in each of the optimization processes. It should be noted that it is possible to increase the device speed by maximizing the x-direction length (given the constant input rotational speed). It was calculated based on the leg foot trajectories obtained through Simscape simulation. Once the trajectories were exported, their minimum and maximum values in the x-axis were found and subtracted. Hence, the first objective function f1(x) was obtained as:

$$f_1(\mathbf{x}) = \Delta x = x_{\max} - x_{\min}. \tag{3}$$

### 2.2.2 Trajectory Height Variation

Trajectory height variation was used as the second objective function and was minimized. Firstly, it

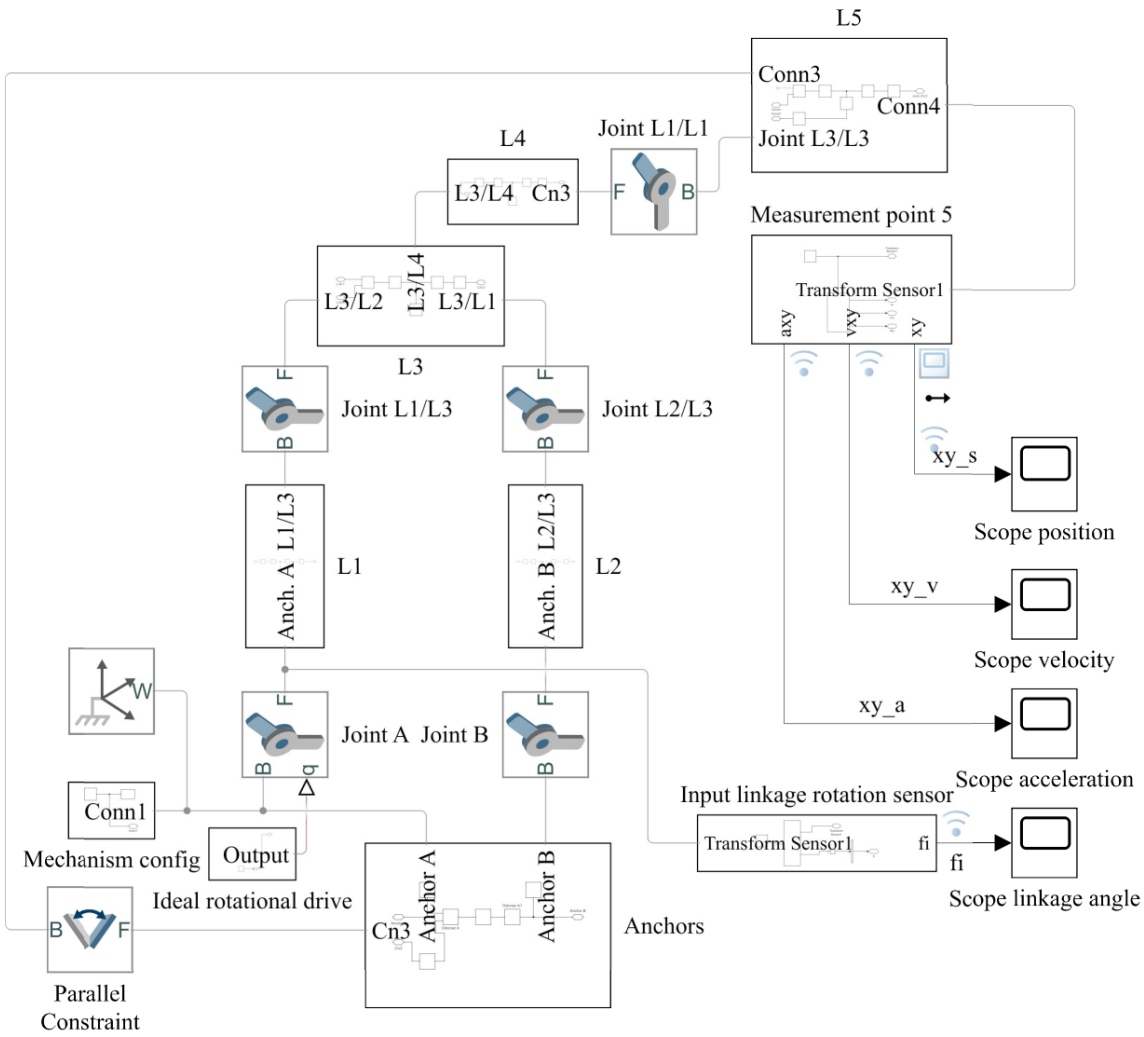


**Fig. 3.** *Simscape simulation schematic*

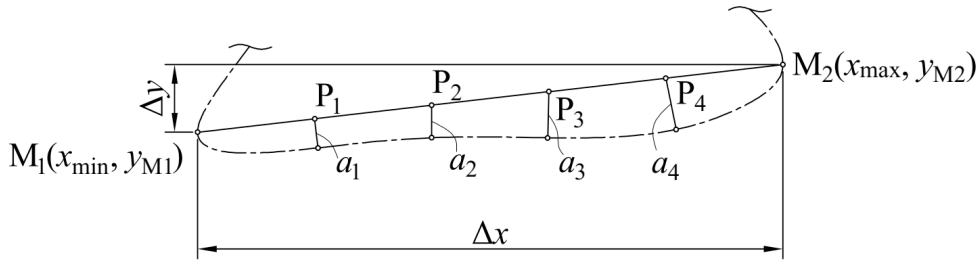


**Fig. 4.** *The trajectory height variation minimization*

was necessary to determine the points outlining the maximum length in the *x*-direction – $M_1(x_{min}, y_{M1})$ and $M_2(x_{max}, y_{M2})$. The trajectory height variation denoted as $H_{var}$ was minimized between $M_1$ and $M_2$ to reduce the changes in the vertical direction (Fig. 4). It was necessary to reduce the change in height between points $M_1$ and $M_2$ (i.e., to reduce $|y_{M1} - y_{M2}|$), as well as to reduce the changes in the *x*-direction length.

Thus, the objective function was created; the difference between $y_{M1}$ and $y_{M2}$ was squared and multiplied by the sum of the distances between points $P_1$, $P_2$, $P_3$, and $P_4$, and the foot trajectory. The difference was squared to emphasize the role of the difference between heights of points $M_1$ and $M_2$ while also ensuring that it will always be positive. Hence, in combination with the distances between the points and the foot trajectory, which are always positive, trajectory height variation will always be positive. Finally, trajectory height variation was expressed as the objective function $f_2(\mathbf{x})$ and minimized:

$$f_2(\mathbf{x}) = H_{var} = (y_{M1} - y_{M2})^2 \cdot \cdot\left[\min(a_1) + \min(a_2) + \min(a_3) + \min(a_4)\right], \quad (4)$$

where *n* denotes the number of discrete points within the interval.

The height variation function presented above has no physical meaning; it is merely a function providing the lowest variations in trajectory height. While the difference between the overall maximum and minimum *y*-axis position is simpler to calculate and can also be used, it would not guarantee steady movement. In this case, the resulting curves had low quality and did not result in an industrially viable mechanism.

#### 2.2.3 Speed Fluctuation

The speed fluctuation was selected as the third objective function. Minimizing the foot speed fluctuation will result in reduced accelerations throughout the cycle. This will, in turn, reduce inertial forces during the cycle, resulting in a smoother operation [19]. In this study, the foot speed fluctuation was taken as:

$$f_3(\mathbf{x}) = \frac{\sum_{i=1}^{n} \left| v_i - v_{avg} \right|}{n}, \quad (5)$$

where *n* is the number of discrete points observed during one cycle (in this article, $n = 3024$), $v_i$ is the resultant speed in each of the points, and $v_{avg}$ is the average speed of all the points.

#### 2.2.4 Maximum Foot Acceleration

While reducing the speed fluctuation will result in a more uniform acceleration during the stride, it will not directly affect its maximum value. However, reducing the maximum foot acceleration will result in a lower maximum inertial force, often used as an input while sizing the drive mechanism. Hence, foot acceleration was used as the fourth objective function. The maximum acceleration was obtained from the Simscape data as a result of *x*-axis and *y*-axis accelerations and was minimized:

$$f_4(\mathbf{x}) = a_{max}. \quad (6)$$

## 3 RESULTS AND DISCUSSION

The optimization processes were carried out for three sets of objective functions according to the method outlined in Section 2. Objective function sets were as follows: length in the *x*-direction and trajectory height variation (set 1), length in the *x*-direction and speed fluctuation (set 2), and length in the *x*-direction and acceleration (set 3). Furthermore, it should be noted that optimization was carried out using a personal computer with an i7-4810MQ processor (2.86 GHz)

and 32 GB of RAM. The time needed to evaluate units from each set was similar, regardless of the objective function, meaning that the Simscape simulation had a significantly higher computational cost compared to NSGA-II operations. The average calculation time was approx. 2 s per unit. Additionally, validation was carried out using set 1 as an example (for more details on the validation, see Section 2.1).

### 3.1 Length Δx and Trajectory Height Variation

The optimization process was first carried out using the length in the *x*-direction and trajectory height variation as objective functions. Four Pareto optimal solutions were obtained, as shown in Fig. 5. The solutions were labelled as "Height" and index ranging between 1 and 4, with lower indices representing larger strides (and higher variations in trajectory height). Hence, the highest *x*-direction length was obtained for Height 1, 584.2 mm, with a height variation value of 955.6. The lowest trajectory variation was obtained for the solution labelled Height 4, 0.01833, with the corresponding $\Delta x = 483.6$ mm.

Compared to other optimization processes (see Sections 3.2. and 3.3.), only four solutions were found on the Pareto front; all remaining final population solutions were dominated by the four solutions presented in Fig. 5. and Table 1.

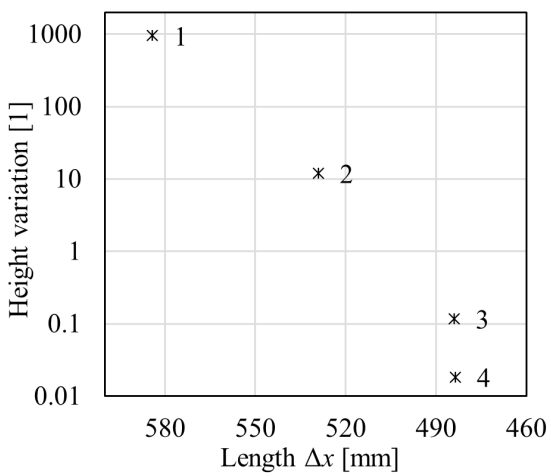


**Fig. 5.** *The x-direction length and height variation*

The range between the extreme Pareto solutions for Δ*x* was 100.6 mm (17.22 % of the highest obtained value). Solution height variations could not be compared in a similar manner as the change was not linear (see fitness function $f_2$). Thus, to better illustrate changes in the height variation and the importance of measurement, strides were plotted for all the Pareto optimal solutions (Fig. 6).

**Table 1.** *Set 1 solutions – values*

| No. | $L_0$ | $L_1$ | $L_2$ | $L_3$ | $L_4$ | $L_5$ |
|---|---|---|---|---|---|---|
| 1 | 180.8 | 108.4 | 237.7 | 234.3 | 272.2 | 1197 |
| 2 | 189.3 | 98.67 | 269.4 | 270.2 | 261.5 | 1150 |
| 3 | 187.9 | 98.97 | 235 | 232.2 | 252.2 | 1232 |
| 4 | 186 | 101.5 | 231.8 | 231 | 237.1 | 1248 |

Linkage lengths measured in mm

As shown in Fig. 6, paths obtained for solutions Height 1 and Height 2, with respective height variation values of 955.6 and 12.03, resulted in a curved bottom segment of the leg trajectory. Since the bottom segment corresponds with the period during which the foot is in contact with the surface, both solutions will require larger torque to operate. Changes in height will require the driver to lift the device body and provide movement in the horizontal direction. In contrast, the bottom trajectory segments of solutions Height 3 and Height 4, with height variations of 0.118 and 0.018, respectively, were remarkably straight. While the variations were slightly more prominent in the Height 3 trajectory, as shown in Fig. 6, it can be concluded that both solutions will not require an increase in required input torque. Moreover, it can be concluded that the height variation of 0.12 is acceptable, but the value is strictly limited to the optimization of similarly sized mechanisms.

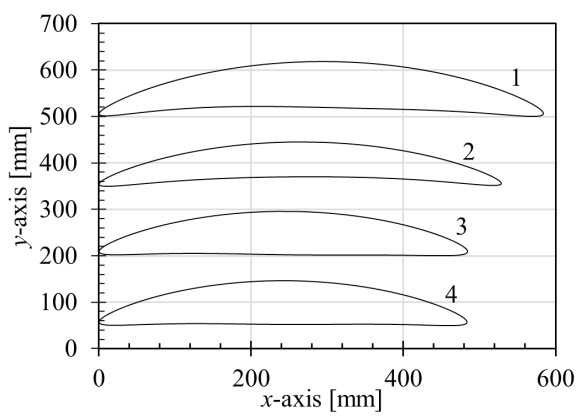


**Fig. 6.** *Foot paths of Pareto optimal solutions*

Finally, none of the variables constituting Pareto optimal solutions were in the vicinity of the design variable range boundaries. Similarly, the same design variables were also not restricted by Grashoff's criterion. Therefore, it was concluded that the selected design variable ranges were appropriate for optimizing

the Chebyshev Lambda mechanism considering the $\Delta x$ length and height variation.

### 3.2 Change in the x-direction and Speed Fluctuation

The optimization process was carried out for the $\Delta x$ length and speed fluctuation along the stride. Solutions on the Pareto front and the associated linkage lengths are provided in Fig. 7 and Table 2. Similarly to Section 3.1, Pareto optimal solutions were indexed from 1 to 11, starting with the solution having the longest $\Delta x$ length. Additionally, the label "Speed" was included before the index. The highest obtained $\Delta x$ was 487.3 mm; the same solution yielded a speed fluctuation of 7426 (Speed 1). On the other side of the Pareto front, the lowest speed fluctuation of 6861 was obtained, for which $\Delta x$ = 464.7 mm (Speed 11).

### 3.3 Change in the x-direction and Acceleration

The $x$-direction length and maximum foot acceleration were selected as the third pair of objective functions. This combination was to provide a mechanism that will result in a steady and fast movement, and the results are presented in Fig. 8 and Table 3. Eleven Pareto optimal solutions were found, labelled as "Acceleration" 1 to 11, with lower indices associated with larger $\Delta x$ values and higher accelerations; the opposite was true for higher indices. The largest $\Delta x$ length of 445.1 mm was obtained for the solution Acceleration 1, corresponding to the highest acceleration between the solutions (122.7 m/s$^2$). In contrast, the lowest acceleration of 117.3 m/s$^2$ was obtained for Acceleration 11 ($\Delta x$ = 432.7 mm). The ranges between the extreme Pareto solutions were

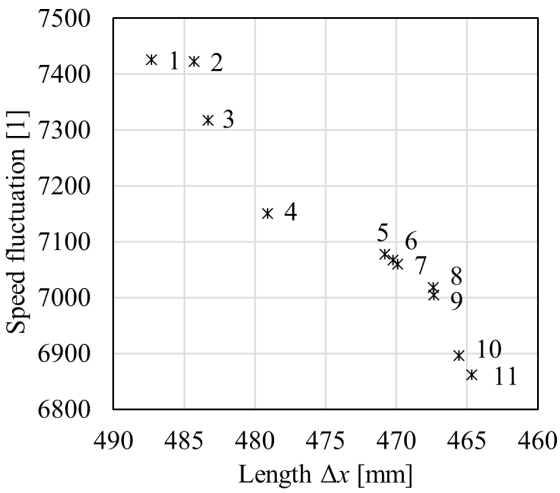


**Fig. 7.** *The x-direction length and speed fluctuation*

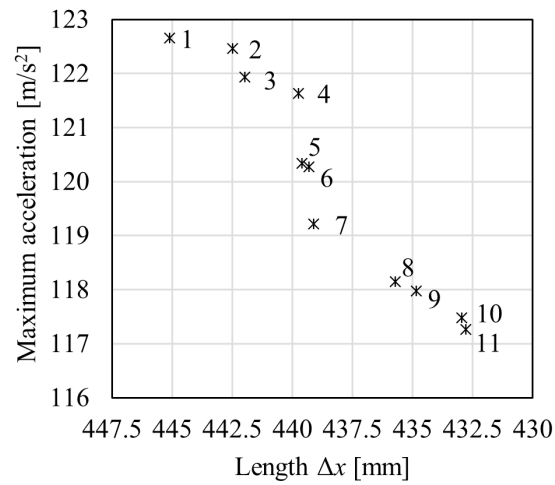


**Fig. 8.** *Length Δx and maximum acceleration*

**Table 2.** *Set 2 solutions – values*

| No. | $L_0$ | $L_1$ | $L_2$ | $L_3$ | $L_4$ | $L_5$ |
|---|---|---|---|---|---|---|
| 1 | 206.4 | 97.18 | 270.2 | 172.5 | 241.5 | 1268 |
| 2 | 206.6 | 97.37 | 272.0 | 177.0 | 240.8 | 1263 |
| 3 | 206.6 | 97.13 | 269.5 | 172.6 | 240.3 | 1271 |
| 4 | 207.3 | 96.44 | 268.6 | 169.6 | 240.0 | 1275 |
| 5 | 191.0 | 90.17 | 252.6 | 160.8 | 234.9 | 1312 |
| 6 | 191.2 | 90.38 | 252.5 | 162.2 | 235.4 | 1310 |
| 7 | 189.6 | 90.16 | 252.5 | 165.0 | 235.0 | 1307 |
| 8 | 191.7 | 90.12 | 251.0 | 159.9 | 235.1 | 1314 |
| 9 | 191.4 | 90.09 | 251.0 | 160.3 | 235.1 | 1314 |
| 10 | 218.6 | 97.95 | 270.2 | 161.3 | 237.8 | 1283 |
| 11 | 217.2 | 97.51 | 271.2 | 164.8 | 238.1 | 1278 |

Linkage lengths measured in mm

**Table 3.** *Set 3 solutions – values*

| No. | $L_0$ | $L_1$ | $L_2$ | $L_3$ | $L_4$ | $L_5$ |
|---|---|---|---|---|---|---|
| 1 | 216 | 90.63 | 250.5 | 157.2 | 265.5 | 1286 |
| 2 | 215.8 | 90.64 | 251.1 | 158.1 | 263.1 | 1287 |
| 3 | 216.5 | 90.67 | 249.8 | 156.1 | 263.4 | 1290 |
| 4 | 216.3 | 91.12 | 249.3 | 159.2 | 263.6 | 1287 |
| 5 | 215.8 | 90.80 | 251.5 | 160.2 | 261.9 | 1286 |
| 6 | 215.8 | 90.83 | 251.4 | 160.7 | 261.9 | 1285 |
| 7 | 216.4 | 90.58 | 249.1 | 156.8 | 263.3 | 1290 |
| 8 | 216 | 90.15 | 251.0 | 159.5 | 261.6 | 1288 |
| 9 | 216.5 | 90.20 | 248 | 156.4 | 262.6 | 1298 |
| 10 | 216.6 | 90.02 | 247.8 | 156.1 | 262.1 | 1294 |
| 11 | 217.3 | 90.13 | 248.8 | 156.8 | 262.1 | 1292 |

Linkage lengths measured in mm

12.34 mm for the $\Delta x$ length (2.77 % of the highest obtained value) and 4.4 m/s$^2$ for the acceleration (4.4 %). Thus, it can be concluded that changes in acceleration were more prominent when observing the Pareto front.

Regarding the variable boundary ranges, the only active condition was for the lower $L_1$ value, which was set to 90 mm. All the Pareto-optimal solutions stemmed toward the lower variable boundary, implying that when aiming to increase the $\Delta x$ length and decrease the foot acceleration, the $L_1$ range should be increased further. The distance between the anchors $L_0$ in optimal solutions ranged between 215.8 mm and 217.3 mm, illustrating a rather low variance. Linkage $L_2$ length was practically equal to the default value, while the lengths of linkages $L_3$ differed the most with respect to the defaults.

Obtained accelerations are theoretical and much higher than their experimental counterparts. This is due to the fixed rotational velocity at the mechanism input. The constant rotational velocity implies infinite torque; in other words, realistic loads stemming from the mechanism operation will not slow down the motor. Hence, high acceleration values were obtained, resulting in significant inertial forces within the system. In a realistic case, if operated via motor, such large accelerations would not occur as the increased inertial forces would slow down the motor.

### 3.4 Comparison to the Default Mechanism

Furthermore, to compare previously obtained Pareto fronts to the default mechanism, its characteristics were determined next. The default mechanism $x$-direction length was 470.4 mm. A trajectory height variation of 0.2799 was also obtained, while the speed fluctuation was 4.32e4. Finally, the maximum acceleration of the default mechanism foot was 2.27e5 m/s$^2$.

The default value was compared to designated solutions from the Pareto optimal fronts for each pair of objective functions, as shown in Fig. 9. The objective function outputs for each of the solutions in the diagram were divided with the corresponding value obtained for the default solution. The only exception was the trajectory height variation, normalized to a [0, 1] interval via min-max normalization supplemented with a logarithmic operator. This was necessary to retain clarity, as the objective function outputs for trajectory height variation were exponential. They were normalized as follows:

$$H'_{\mathrm{var}\,i} = \frac{\log H_{\mathrm{var}\,i} - \min\left(\log H_{\mathrm{var}}\right)}{\max\left(\log H_{\mathrm{var}}\right) - \min\left(\log H_{\mathrm{var}}\right)}. \quad (7)$$

As shown in the figure, solutions obtained while optimizing for length $\Delta x$ and trajectory height variation (Height 1 and 4) yielded larger values than the default solution. While Height 1 $\Delta x$ was significantly larger compared to the default solution, so was its height variation. In contrast, Height 4 $\Delta x$ was 13.2 mm longer, having lower height variation, speed fluctuation, and slightly higher maximum acceleration. Compared to other solutions (barring Height 4), the default one had a significantly lower trajectory height variation. Thus, it is recommended to include the height variation as a boundary condition when designing a walking mechanism.

Moreover, when considering the speed fluctuation criterion, the default solution resulted in the second-highest value (behind the Height 1 solution). Solutions

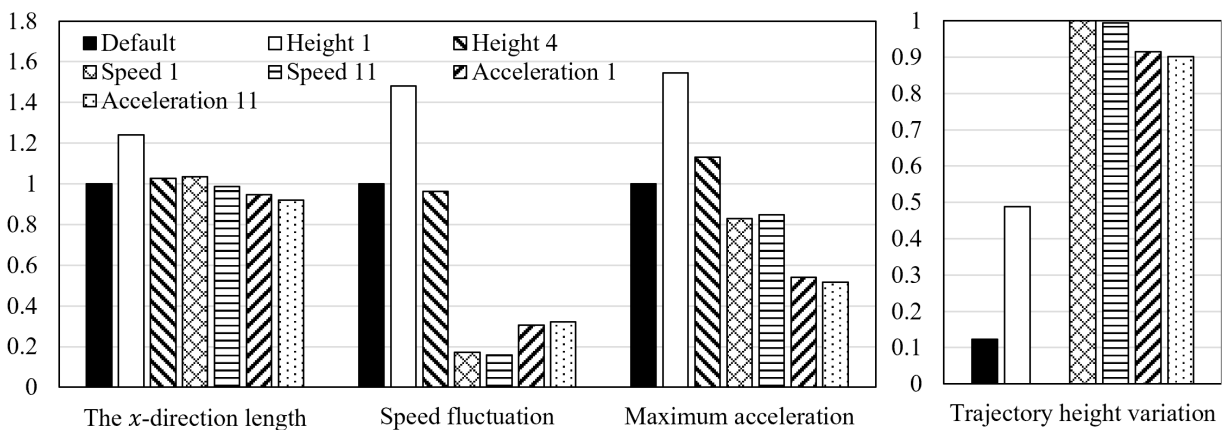


**Fig. 9.** *Comparison between the default and optimal solutions*

obtained when minimizing the acceleration had a low-speed fluctuation, as expected. Similarly, solutions obtained when aiming to reduce the speed fluctuation (Speed 1 and Speed 11, for more details, see Section 3.2.) resulted in low maximum acceleration values. Such behaviour was expected, as speed fluctuation and maximum acceleration are linked indirectly.

Finally, it should be clarified that in Fig. 9, a higher $\Delta x$ length is considered positive, while higher speed fluctuation, maximum acceleration, and trajectory height variation values imply a lower-quality solution. Moreover, in the trajectory height variation graph, the solution Height 4 column is missing; it had the lowest value of all the seven observed solutions and was normalized to 0.

## 4 CONCLUSIONS

The procedure for multi-objective optimization of walking mechanisms based on the Simscape Simulation embedded within the NSGA-II was presented. The simplest of the mechanisms, the Chebyshev Lambda mechanism, was used as an example and was optimized. The proposed method also applies to both 6-bar and 8-bar linkages, with slight differences in integration. A new computer-aided design (CAD) model should be created, and corresponding design variables and boundary conditions should be selected.

The variable ranges were set based on the default mechanism, and Grashoff's criterion was used to ensure that the resultant solutions would be viable. Optimal solutions were found for three pairs of objective functions: $\Delta x$ length/height variation, $\Delta x$ length/speed fluctuation, and $\Delta x$ length/maximum foot acceleration. Based on the presented results, the following conclusions were made:

- The presented procedure enabled a timely and comprehensive analysis of the candidate mechanisms; the calculation time was approximately 2 s per unit.
- Considering the length in the $x$-direction and height variation, notable advancements were made. For the Pareto optimal solution with the highest length, the increase with respect to the default solution was 24.2 %. Moreover, all the Pareto optimal solutions had higher $\Delta x$ lengths than the default solution.
- It is recommended to introduce the trajectory height variation as a boundary condition when aiming to use the Chebyshev Lambda mechanism as a walking mechanism.

However, the limitations of the presented study should be addressed as well. The proposed method considers the walking mechanism without taking into account its surroundings. A device utilizing walking mechanisms for movement will include multiple such mechanisms; hence, influences of operating conditions and gaits (e.g., biped, quadruped, hexapod) should also be considered. Furthermore, when using the results of this study, it is necessary to acknowledge that a minimal number of boundary conditions was used as the authors primarily observed the effects of objective functions on the solution characteristics. Hence, some of the Pareto solutions would result in sub-optimal walking mechanisms due to variations in length in the $x$-direction.

For this reason, in the future study, we plan to generate a mechanism through multi-objective optimization by simultaneously introducing all the objective functions (instead of pairs, which were considered here). Finally, it should be added that this study only considered the mechanism kinematics; hence, the viability of the optimal mechanism should be verified by either simulating its dynamics or experimentally.

## 5 REFERENCES


[1] Wu, J., Yao, Y. (2018). Design and analysis of a novel walking vehicle based on leg mechanism with variable topologies. *Mechanism and Machine Theory*, vol. 128, p. 663-681, **DOI:10.1016/j.mechmachtheory.2018.07.008**.

[2] Kulandaidaasan Sheba, J., Elara, M., Martínez-García, E., Tan-Phuc, L. (2016). Trajectory generation and stability analysis for reconfigurable Klann mechanism based walking robot. *Robotics*, vol. 5, no. 3, art. ID. 13, **DOI:10.3390/robotics5030013**.

[3] Singh, R., Bera, T.K. (2020). Walking model of Jansen mechanism-based quadruped robot and application to obstacle avoidance. *Arabian Journal for Science and Engineering*, vol. 45, p. 653-664, **DOI:10.1007/s13369-019-04135-8**.

[4] Kim, H., Jeong, K., Seo, T. (2017). Analysis and experiment on the steering control of a water-running robot using hydrodynamic forces. *Journal of Bionic Engineering*, vol. 14, p. 34-46, **DOI:10.1016/S1672-6529(16)60376-1**.

[5] Komoda, K., Wagatsuma, H. (2017). Energy-efficacy comparisons and multibody dynamics analyses of legged robots with different closed-loop mechanisms. *Multibody System Dynamics*, vol. 40, p. 123-153, **DOI:10.1007/s11044-016-9532-9**.

[6] Nansai, S., Elara, M.R., Iwase, M. (2013). Dynamic analysis and modeling of Jansen mechanism. *Procedia Engineering*, vol. 64, p. 1562-1571, **DOI:10.1016/j.proeng.2013.09.238**.

[7] Sheba, J.K., Martinez-Garcia, E., Elara, M.R., Tan-Phuc, L. (2015). Design and evaluation of reconfigurable Klann mechanism based four legged walking robot. *10th International*

*Conference on Information, Communications and Signal Processing*, p. 1-5, **DOI:10.1109/ICICS.2015.7459939**.

**[8]** Kim, H., Lee, S., Lim, E., Jeong, K., Seo, T. (2016). Comparative study of leg mechanisms for fast and stable water-running. *International Journal of Precision Engineering and Manufacturing*, vol. 17, p. 379-385, **DOI:10.1007/s12541-016-0047-3**.

**[9]** Sheba, J.K., Rajesh, M., Mart, E., Tan-phuc, L. (2017). Synthesizing reconfigurable foot traces using a Klann mechanism. *Robotica*, vol. 35, no. 1, p. 189-205, **DOI:10.1017/S0263574715000089**.

**[10]** Nansai, S., Rojas, N., Elara, M.R., Sosa, R., Iwase, M. (2015). On a Jansen leg with multiple gait patterns for recon-figurable walking platforms. *Advances in Mechanical Engineering*, vol. 7, no. 3, **DOI:10.1177/1687814015573824**.

**[11]** Desai, S.G., Annigeri, A.R., TimmanaGouda, A. (2019). Analysis of a new single degree-of-freedom eight link leg mechanism for walking machine. *Mechanism and Machine Theory*, vol. 140, p. 747-764, **DOI:10.1016/j.mechmachtheory.2019.06.002**.

**[12]** Erkaya, S. (2013). Trajectory optimization of a walking mechanism having revolute joints with clearance using ANFIS approach. *Nonlinear Dynamics*, vol. 71, p. 75-91, **DOI:10.1007/s11071-012-0642-5**.

**[13]** Wei, C., Sun, H., Liu, R., Yao, Y., Wu, J., Liu, Y., Lu, Y. (2022). Analysis and experiment of thrust-propelled closed-chain legged platform with passive locomotion ability. *Mechanism and Machine Theory*, vol. 167, art. ID 104506, **DOI:10.1016/j.mechmachtheory.2021.104506**.

**[14]** Deb, K., Pratap, A., Agarwal, S., Meyarivan, T. (2002). A fast and elitist multi-objective genetic algorithm: NSGA-II. *IEEE Transactions on Evolutionary Computation*, vol. 6, no. 2, p. 182-197, **DOI:10.1109/4235.996017**.

**[15]** Miler, D., Hoić, M., Škec, S., Žeželj, D. (2020). Optimisation of polymer spur gear pairs with experimental validation. *Structural and Multidisciplinary Optimization*, vol. 62, p. 3271-3285, **DOI:10.1007/s00158-020-02686-1**.

**[16]** Zhang, P., Qian, Y., Qian, Q. (2021). Multi-objective optimization for materials design with improved NSGA-II. *Materials Today Communications*, vol. 28, art. ID 102709, **DOI:10.1016/j.mtcomm.2021.102709**.

**[17]** Miler, D., Hoić, M. (2021). Optimisation of cylindrical gear pairs: A review. *Mechanism and Machine Theory*, vol. 156, art. ID 104156, **DOI:10.1016/j.mechmachtheory.2020.104156**.

**[18]** Ghaderian, M., Veysi, F. (2021). Multi-objective optimization of energy efficiency and thermal comfort in an existing office building using NSGA-II with fitness approximation: A case study. *Journal of Building Engineering*, vol. 41, art. ID 102440, **DOI:10.1016/j.jobe.2021.102440**.

**[19]** Ingram, A.J. (2006). *A New Type of Mechanical Walking Machine* (PhD thesis). University of Johannesburg, Johannesburg.